



A two-scale model for subcritical damage propagation

Cristian Dascalu *, Bertrand François, Oumar Keita

Laboratoire Sols Solides Structures – Risques, UJF, INPG, CNRS UMR 5521, Domaine Universitaire, B.P. 53, 38041 Grenoble Cedex 9, France

ARTICLE INFO

Article history:

Received 23 July 2009

Received in revised form 14 October 2009

Available online 23 October 2009

Keywords:

Micro-cracks

Subcritical propagation

Homogenization

Time-dependent damage

Relaxation

Creep

Size effect

ABSTRACT

The failure behaviour of quasi-brittle materials is often time-dependent. This dependence is due to physical processes taking place at the level of the micro-structure. For a rigorous modeling of the time-dependent behaviour of that kind of solids, a two-scale approach is well suited. This paper investigates time-dependent damage which microscopic origin is the subcritical micro-crack growth. We present a two-scale time-dependent damage model completely deduced from small-scale descriptions of subcritical micro-crack propagation, without any macroscopic assumptions. The passage from the micro-scale to the macro-scale is done through an asymptotic homogenization approach. At the micro-scale, the tensile failure due to the subcritical propagation of cracks is the dominant mechanism of creep observed at the macro-scale. We consider microstructures with cracks evolving in different subcritical regimes. We assume a complex propagation law that considers three characteristic regimes of subcritical crack growth, corresponding to different physical processes at the crack tip level. Numerical simulations of constant strain rate, relaxation and creep tests illustrate the ability of the developed model to reproduce different regimes of time-dependent damage response.

© 2009 Elsevier Ltd. All rights reserved.

1. Introduction

The problem of distributed subcritical failure must be accurately treated for many applications dealing with the mechanics of quasi-brittle materials such as glasses, rocks, ceramics or ceramic composites. A subcritical criterion of crack propagation considers that crack may grow for energy lower than the critical limit of fracture. The rate of crack propagation is usually related to the stress intensity factor at the crack tips, under mode I (tensile mode). At the micro-scale, the tensile failure due to the subcritical propagation of cracks may represent the main micro-mechanism of creep observed at the macro-scale. This effect can be observed in many different materials such as rocks, ceramics or glasses (Miura et al., 2003; Main, 2000; Nara and Kaneko, 2006; Munt and Fett, 2001).

The constitutive modeling of the time effect on the mechanical damage behaviour of materials (Betten, 2002; Cristescu and Hunsche, 1998; Lemaitre and Desmorat, 2005) can be addressed according to two distinct approaches: (i) the phenomenological models are based on internal variables, having empirical characters for most of them, that are calibrated to fit with experimental observations (Challamel et al., 2005; Pietruszczak et al., 2004), (ii) the micromechanics-based approaches are able to capture the physical micro-mechanisms that produce damage and irreversible deformations which are partially or totally time-dependent. From

such micro-scale considerations, Abou-Chakra Guery et al. (2009) developed a model for argillite assuming it as a three-phase composite subject to viscous and damage effects. Also Nadot et al. (2006) (see also Dartois et al. (2009)) developed a viscoelastic damage model via a scale transition approach in which damage occurs by grain/matrix debonding.

Experimental observations of fracture propagation (e.g. Anderson and Grew, 1977; Meredith and Atkinson, 1985) indicate that the dependence of fracture propagation rate on the stress intensity factor in mode I can generally be approximated by a trimodal behaviour (Fig. 1). In region I, the rate of stress corrosion reaction control the velocity of the crack growth. The plateau of region II is mainly determined by the rate of transport of reactive species to crack tips. In region III, the drastic increase of the velocity of crack growth up to failure is relatively independent of the chemical environment and is controlled by mechanical rupture (Freiman, 1984; Atkinson and Meredith, 1987). This typical three-mode regime is characteristics of glasses, ceramics or rocks but is less marked in metals. In most of the approaches studying the subcritical propagation of cracks, this complex trimodal behaviour is often approximated by a single mode. This approximation may be done if the behaviour of the material is studied in a restricted range of stress intensity factor, limiting the study in one of the three regions. On the contrary, for a complete modeling of the problem, from crack initiation to coalescence of cracks upon failure, the three regions must be considered.

Previous attempts to make a link between subcritical propagation of micro-cracks and the macroscopic damage behaviour are

* Corresponding author.

E-mail address: Cristian.Dascalu@hmg.inpg.fr (C. Dascalu).

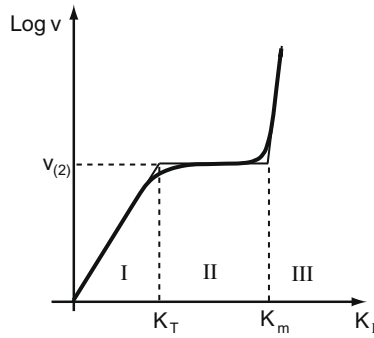


Fig. 1. Velocity of the crack propagation versus the stress intensity factor. The three regions are separated by the two characteristic stress intensity factors: K_T and K_m . The bold line corresponds the composite law (Eq. (11)).

very few, e.g. the micromechanical analysis in Okui and Horii (1997) and Miura et al. (2003). The novelty of the present approach is many-fold: (i) the new subcritical damage model accounts, through a compact form of the damage law, for the three regimes of failure described previously; (ii) it appears to be the first subcritical model of damage deduced through the mathematical homogenization method based on asymptotic developments; and (iii) the subcritical damage laws allow for predictions of size effects.

Experimental evidences on the trimodal character of the subcritical crack propagation are, most of the time, found at the laboratory scale (through Double Torsion Test, for instance). For applications to geomechanics and geophysics, this scale may be considered as the microscopic scale. As observed by Scholz (1972), the macroscopic rock creep is related to the growth of microfissures by stress corrosion cracking that may create delayed triggering of earthquakes. In aluminium alloys, Ruckert et al. (2006) have shown that, within a limited range of stress intensity factor, very good similarity has been obtained between micro- and macroscopic rates of crack growth. One may expect that subcritical growth take place for micro-cracks at smaller scales. These observations motivate the consideration of the subcritical growth of microscopic cracks as one of the origins of the time-dependent damage behaviour.

A two-scale approach for damage was deduced in Dascalu et al. (2008) and Dascalu and Bilbie (2007) for brittle damage. A more general formulation of this model, including non-brittle behaviours, was recently given in Dascalu (2009) and a model accounting for mixed-mode fracture in compression was developed in François and Dascalu (submitted for publication). The main objective of the present contribution is to deduce a damage model from a micromechanical description of subcritical crack propagation in tension and that accounts for the three regimes of failure.

We assume that micro-crack propagation follows an exponential-type multi-regime subcritical law and we use homogenization to obtain a macroscopic time-dependent damage model. The passage from the micro-scale to the macro-scale is done through the asymptotic homogenization approach (e.g. Benssousan et al., 1978; Sanchez-Palencia, 1980).

The paper is organized as follows. First, the three-regime subcritical propagation law is discussed. Then, the mathematical formulation of the two-scale problem is presented and the macroscopic damage equations are deduced through the asymptotic homogenization procedure. Finally, the ability of the model to reproduce known time-dependent behaviours for constant strain rate, relaxation and creep tests is demonstrated by means of numerical simulations of the local homogenized response.

2. Subcritical crack growth

Classical fracture mechanics postulates that in a linear elastic body an isolated crack under tensile loading will propagate in the medium once a critical mode I stress intensity factor, K_{IC} , has been reached or exceeded, while for lower values of K_I the propagation is not possible. The subcritical criterion considers that crack propagation is time-dependent and may occur for stress intensity factor lower than the critical limit of fracture (Atkinson and Meredith, 1987).

The most commonly used equations to describe the relation between subcritical crack growth and stress intensity factor in mode I, K_I , are the power law (Charles, 1958)

$$v = V_1 (K_I)^n \quad (1)$$

and the exponential law (Wiederhorn and Bolz, 1970)

$$v = V_2 \exp(-c + bK_I) \quad (2)$$

where V_1 , V_2 , n , b and c are positive constants. The distinction between the performance of the predictions of Eqs. (1) and (2) to describe subcritical crack growth is often impossible. The range of variation of K_I in the experimental data are generally limited which makes that both power and exponential laws fit with observations. However, outside of the range of experimental observations the predictions of these two constitutive equations may diverge significantly. Moreover, the previous equations are only valid in a given region of the trimodal response of the material (Fig. 1), generally in region I, which makes impossible the simulation of advanced stages of material rupture (characteristic of region III).

From consideration of atomic theories and reaction rate theories of crack propagation (including stress corrosion, dissolution, diffusion, ion-exchange and microplasticity), it is possible to relate the empirical coefficients of Eqs. (1) and (2) with physical characteristics of the microstructure. Considering crack growth as a succession of water vapor enhanced rupture of small material element immediately adjacent to the crack tips, Salganik et al. (1997) showed that the three regimes of crack propagation can be predicted, respectively, by the three following equations:

$$v_{(1)} = \frac{v_0 \phi_0^n}{n} \exp \left(-\frac{U'_{01} - \Omega'_1 K_I / \sqrt{2\pi d_m}}{kT} \right) \quad (3)$$

$$v_{(2)} = \frac{b_0 p}{N_A n \sqrt{2\pi m k T}} \quad (4)$$

$$v_{(3)} = \frac{d_m}{\tau_0} \exp \left(-\frac{U'_{03} - \Omega'_3 K_I / \sqrt{2\pi d_m}}{kT} \right) \quad (5)$$

where T is the absolute temperature, k is Boltzmann's constant, Ω'_1 is a stress sensitivity factor, $\tau_0 \approx 10^{-12} - 10^{-13}$ s is a typical period of atomic fluctuations, ϕ_0 is the relative concentration of water in the gas next to the crack tips, n is the number of molecules of water required for the water-assisted rupture of a single bridging bond, d_m is the length of the material structure, b_0 is the bridging bond length, N_A is the Avogadro number, v_0 is the mean velocity of diffusion, m is the molecular mass of water, p is the partial pressure of water vapor, U'_{01} and U'_{03} are the zero stress activation energy in regions I and III, respectively, and Ω'_1 and Ω'_3 are stress sensitivity factors in regions I and III. Numerical values of those parameters are reported in Table 1.

Grouping the material and environmental constants by posing: $a = \frac{v_0 \phi_0^n}{n} \exp \left(-\frac{U'_{01}}{kT} \right)$, $b = \frac{b_0 p}{N_A n \sqrt{2\pi m k T}}$, $c = \frac{d_m}{\tau_0} \exp \left(-\frac{U'_{03}}{kT} \right)$, $S_1 = \frac{\Omega'_1}{\sqrt{2\pi d_m k T}}$ and $S_3 = \frac{\Omega'_3}{\sqrt{2\pi d_m k T}}$, we obtain the following expressions:

Table 1

Material parameters used in the simulations.

E (Pa)	ν	ε (m)	T (K)	n	ϕ_0	U'_{01} (J)
2×10^9	0.3	10^{-2}	325	1	6.32×10^{-10}	2×10^{-19}
d_m (m)	τ_0 (s)	U'_{03} (J)	$v_{(2)}$ (m/s)	v_0 (m/s)	Ω'_1 (J)	Ω'_3 (J)
25×10^{-4}	10^{-12}	2×10^{-18}	10^{-8}	9×10^4	1.27×10^{-23}	8.28×10^{-24}

$$v_{(1)} = a \exp(S_1 K_1) \quad (6)$$

$$v_{(2)} = b \quad (7)$$

$$v_{(3)} = c \exp(S_3 K_1) \quad (8)$$

The three regions are delimited by two characteristic stress intensity factors K_T and K_m that can be analytically determined according to the K_I – ν equations (6)–(8) of each region:

$$K_T = \frac{1}{S_1} \ln \left(\frac{b}{a} \right) \quad (9)$$

$$K_m = \frac{1}{S_3} \ln \left(\frac{b}{c} \right) \quad (10)$$

The three distinct velocities (Eqs. (6)–(8)) corresponding to the three regimes of crack propagation can be composed in a unique rate of propagation through the following approximate relationship (Salganik et al., 1997):

$$\nu = \frac{v_{(1)} v_{(2)}}{v_{(1)} + v_{(2)}} + v_{(3)} \quad (11)$$

According to the value of K_I with respect to K_T and K_m , ν takes the value $v_{(1)}$ when $K_I < K_T < K_m$ (i.e. $v_{(3)} \ll v_{(1)} \ll v_{(2)}$), the value $v_{(2)}$ when $K_T < K_I < K_m$ (i.e. $v_{(3)} \ll v_{(2)} \ll v_{(1)}$) or the value $v_{(3)}$ when $K_T < K_m < K_I$ (i.e. $v_{(2)} \ll v_{(1)} \ll v_{(3)}$). A generic form of the composite velocity given by the relation (11) is represented in Fig. 1.

This trimodal behaviour of the micro-crack propagation has several consequences in term of the predicted macroscopic time-dependent response of materials. (i) In region I, the relation between velocity of crack propagation (ν) and the stress intensity factor (K_I) is logarithmic. It means that ν can never be equal to zero, even for low value of K_I . So, in theory, for periods of time tending to infinity, the material damage may increase even at very low stress (or strain) level. (ii) The plateau of region II induces a ductile behaviour of material. In that region, the stress intensity factor (related to the loading level) may increase without producing an acceleration of crack propagation. (iii) On the contrary, region III, attainable for high loading level, is characterized by a brittle rupture of materials.

3. Two-scale problem

In this paper, we consider the quasi-static elasto-damage evolution of the material body. At a given instance of time, the problem is that of an elastic body containing a large number of micro-cracks. We suppose that the micro-crack distribution is locally periodic. Each crack is assumed to be horizontal (parallel to the x_1 -axis), straight and of length l . The damage variable d is defined as the ratio $d = \frac{l}{\varepsilon}$ between the crack length l and the distance between the centers of neighbor micro-cracks ε or, equivalently, the size of a periodicity cell (see Fig. 2a).

3.1. Equilibrium problem

We consider the instantaneous equilibrium of the initial heterogeneous medium, that we assume to be a two-dimensional isotropic elastic medium containing a locally periodic array of micro-cracks. In the solid part $\mathcal{B}_s = \mathcal{B} \setminus \mathcal{C}$, where \mathcal{B} is the whole body and \mathcal{C} the union of all micro-cracks inside \mathcal{B} , the momentum equilibrium is

$$\frac{\partial \sigma_{ij}^e}{\partial x_j} = 0, \quad \text{in } \mathcal{B}_s \quad (12)$$

and the linear elasticity constitutive relation is

$$\sigma_{ij}^e = a_{ijkl} e_{xkl}(\mathbf{u}^e) \quad (13)$$

where a_{ijkl} is the elasticity tensor. σ_{ij}^e is the stress field and \mathbf{u}^e the displacement field from which the strain tensor is deduced in the small deformation hypothesis

$$e_{xij}(\mathbf{u}^e) = \frac{1}{2} \left(\frac{\partial u_i^e}{\partial x_j} + \frac{\partial u_j^e}{\partial x_i} \right) \quad (14)$$

On the crack faces, traction free conditions are assumed:

$$\sigma^e \mathbf{N} = 0 \quad (15)$$

where \mathbf{N} is a unit normal vector on the crack faces.

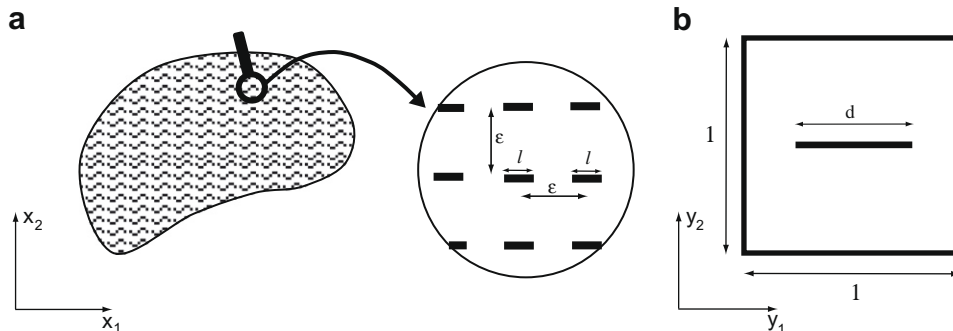


Fig. 2. (a) Micro-fissured medium with locally periodic microstructure, ε is the size of a period and l is the local micro-crack length. (b) Unit cell with rescaled crack of length d .

3.2. Asymptotic homogenization

The locally periodic microstructure is constructed from a reference unit cell Y (Fig. 2b) referred to microscopic coordinates (y_1, y_2) . Rescaled with the small parameter ε , the unit cell becomes the physical period of the material εY . We assume that the microstructural length ε is small enough with respect to the characteristic dimension of the whole body, so that to distinguish between microscopic and macroscopic variations. These variations of mechanical fields at different scales are represented by distinct variables: \mathbf{x} the macroscopic variable and $\mathbf{y} = \mathbf{x}/\varepsilon$ the microscopic variable.

The unit cell Y contains the rescaled crack CY and $Y_s = Y \setminus CY$ its solid part. Following the method of asymptotic homogenization (e.g. Benssousan et al., 1978; Sanchez-Palencia, 1980), we look for expansions of \mathbf{u}^ε and σ^ε in the form

$$\mathbf{u}^\varepsilon(\mathbf{x}, t) = \mathbf{u}^{(0)}(\mathbf{x}, \mathbf{y}, t) + \varepsilon \mathbf{u}^{(1)}(\mathbf{x}, \mathbf{y}, t) + \varepsilon^2 \mathbf{u}^{(2)}(\mathbf{x}, \mathbf{y}, t) + \dots \quad (16)$$

$$\sigma^\varepsilon(\mathbf{x}, t) = \frac{1}{\varepsilon} \sigma^{(-1)}(\mathbf{x}, \mathbf{y}, t) + \sigma^{(0)}(\mathbf{x}, \mathbf{y}, t) + \varepsilon \sigma^{(1)}(\mathbf{x}, \mathbf{y}, t) + \dots \quad (17)$$

where $\mathbf{u}^{(i)}(\mathbf{x}, \mathbf{y}, t)$, $\sigma^{(i)}(\mathbf{x}, \mathbf{y}, t)$, $\mathbf{x} \in \mathcal{B}_s$, $\mathbf{y} \in Y$ are smooth functions and Y -periodic in \mathbf{y} .

Based on previous works (Leguillon and Sanchez-Palencia, 1982; Sanchez-Palencia, 1980), it can be shown that the substitution of Eqs. (16) and (17) in the set of expressions (12)–(15), leads to boundary value problems for the different orders of ε , formulated on the unit cell Y . It can be proved that the function $\mathbf{u}^{(0)} = \mathbf{u}^{(0)}(\mathbf{x}, t)$ is independent of \mathbf{y} variable, representing the macroscopic displacement field.

For given $\mathbf{u}^{(0)}(\mathbf{x}, t)$, for traction-free cracks, we deduce (Leguillon and Sanchez-Palencia, 1982; Sanchez-Palencia, 1980) the following boundary-value problem for the function $\mathbf{u}^{(1)}$:

$$\frac{\partial}{\partial y_j} (a_{ijkl} e_{ykl}(\mathbf{u}^{(1)})) = 0, \quad \text{in } Y_s \quad (18)$$

$$a_{ijkl} e_{ykl}(\mathbf{u}^{(1)}) N_j = -a_{ijkl} e_{xkl}(\mathbf{u}^{(0)}) N_j, \quad \text{on } CY \quad (19)$$

and with periodicity boundary conditions on the external boundary of the cell.

The microscopic correction $\mathbf{u}^{(1)}$ has a linear dependence of the macroscopic deformations: $\mathbf{u}^{(1)}(\mathbf{x}, \mathbf{y}, t) = \xi^{pq}(\mathbf{y}) e_{xpq}(\mathbf{u}^{(0)})(\mathbf{x}, t)$. Here, the characteristic functions $\xi^{pq}(\mathbf{y})$ are elementary solutions of (18) and (19), for the particular macroscopic deformations $e_{xpq}(\mathbf{u}^{(0)}) = \delta_{pq}$.

By introducing the mean value operator $\langle \cdot \rangle = \frac{1}{|Y|} \int_{Y_s} \cdot d\mathbf{y}$, where $|Y|$ is the area of Y , we can prove (Leguillon and Sanchez-Palencia, 1982; Dascalu et al., 2008) that the macroscopic stress is

$$\Sigma_{ij}^{(0)} \equiv \langle \sigma_{ij}^{(0)} \rangle = C_{ijkl}(d) e_{xkl}(\mathbf{u}^{(0)}) \quad (20)$$

as a function of the macroscopic strain $e_x(\mathbf{u}^{(0)})$ where $\sigma_{ij}^{(0)} = a_{ijkl}(e_{xkl}(\mathbf{u}^{(0)}) + e_{ykl}(\mathbf{u}^{(1)}))$ and

$$C_{ijkl}(d) = \frac{1}{|Y|} \int_{Y_s} (a_{ijkl} + a_{ijmn} e_{ymn}(\xi^{kl})) d\mathbf{y} \quad (21)$$

are the homogenized coefficients. The effective constitutive relation (20) should be used in the macroscopic equilibrium equation which can be deduced in the form (e.g. Sanchez-Palencia, 1980):

$$\frac{\partial}{\partial x_j} (C_{ijkl}(d) e_{xkl}(\mathbf{u}^{(0)})) = 0 \quad (22)$$

Although it is not our intention to consider the influence of the crack orientations but to focus on the determination of a complex damage law for a particular crack direction, we note that the previous formulae are valid for every crack orientation in the periodicity cell. If we denote by θ the angle made by the crack line with

the horizontal direction, then the effective coefficients are functions of d and θ : $C_{ijkl} = C_{ijkl}(d, \theta)$. The couple (d, θ) completely characterizes the state of damage at a given macroscopic point.

These coefficients C_{ijkl} can be computed by solving the unit cell problems (18) and (19) for every d , the crack line being assumed horizontal. In what follows, we consider that the elastic solid matrix is isotropic, of elastic constants E and ν . For given couple (E, ν) , the coefficients can be computed for a large number of $d \in [0, 1]$ and, by interpolation, we can have polynomial expressions of $C_{ijkl}(d)$. For this, polynomials of degree 5 have been used.

The FEAP finite element code (Taylor, 2008) has been used for the computation of these homogenized coefficients. They are represented in Fig. 3 as a function of the damage variable d . The presence of the micro-cracks leads to induced anisotropy, the resulting effective elastic response being orthotropic. We also note the non-linear dependence of the homogenized coefficients on the damage variable d . With an horizontal crack line (direction 11), the loss of rigidity with the damage variable increase is maximum when the unit cell is loaded in the vertical direction (22), i.e. perpendicular to the crack (coefficients C_{2222} and C_{1122}) while the rigidity is much less affected when loaded in the horizontal direction (11), i.e. parallel to the crack (coefficient C_{1111}). This is characteristic of the damage-induced anisotropy observed at the macro-scale.

For $d = 1$, the residual value of C_{2222} and C_{1122} is not zero because the micro-crack tips are assumed to remain in contact, even for fully damaged state. It produces a residual rigidity of the unit cell. It explains that, in the numerical simulations (Section 5), the strain-controlled tests end up with a residual stress value.

4. Damage equations

The effective constitutive law presented in the previous section enables us to compute the stress–strain behaviour of the material at a given state of non-evolving damage. In this section, we consider the evolution of micro-cracks and we deduce the corresponding macroscopic evolution of damage.

Our objective is to deduce the equations characterizing the elasto-damage evolution around a macroscopic point. Under a given loading of the macroscopic structure, the resulting local state of stress leads to the activation of particular families of micro-cracks. In what follows, we place ourselves in such a macroscopic point and we assume that in a small vicinity a family of straight micro-cracks is activated and they are propagating in mode I, symmetrically with respect to their middle-point. Their evolution will be described by the composed subcritical law of propagation (11).

To deduce the macroscopic damage equations we will follow the method developed in Dascalu et al. (2008) and Dascalu (2009). Let us denote the microscopic energy-release rate \mathcal{G}_e , which depends on the crack length l . The micro-crack propagation is described by the following relation:

$$\dot{l} = \bar{v}(\mathcal{G}_e) \quad (23)$$

In our particular case, \bar{v} is given by (11), when expressed in terms of the energy release rate. This relation should be completed with the reduced dissipation inequality:

$$\mathcal{D}_f \equiv \mathcal{G}_e \dot{l} \geq 0 \quad (24)$$

Eqs. (23) and (24) present the general criterion of time-dependent crack propagation at the micro-scale. For brittle fracture, the Griffith criterion can be considered: $\dot{l} = 0$ when $\mathcal{G}_e < \mathcal{G}_f$ and $\dot{l} \geq 0$ when $\mathcal{G}_e = \mathcal{G}_f$, where \mathcal{G}_f is the critical fracture energy of the material. This case was considered in Dascalu et al. (2008) where a brittle damage model has been deduced. For more complex fracture evolutions, \mathcal{G}_f may be a function of the crack length l and the crack speed \dot{l} (e.g. Freund, 1998). Such general fracture laws have been considered in

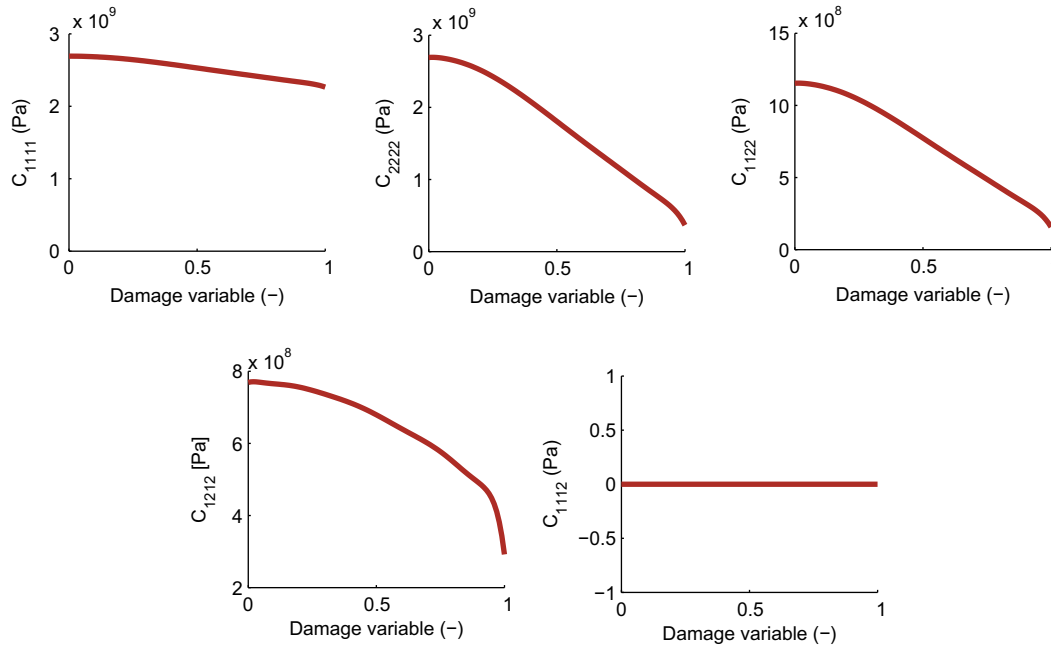


Fig. 3. Homogenized coefficients for horizontal crack orientation for elastic parameters $E = 2$ GPa and $\nu = 0.3$.

Dascalu (2009), where a general damage model has been obtained by homogenization. In our particular case, the relation (23) corresponds to a critical fracture energy \mathcal{G}_f that depends on the crack velocity \dot{l} .

Our subcritical propagation law $\dot{l} = v(K_I)$, where the function $v(K_I)$ is given by (11), can be written in terms of fracture energy by using the relation between the stress intensity factor and the energy release rate, for the mode I propagation:

$$\mathcal{G}_\varepsilon = \frac{1 - \nu^2}{E} (K_I)^2 \quad (25)$$

It was proved in Dascalu et al. (2008) that, for evolving micro-cracks, we have

$$\frac{\mathcal{G}_\varepsilon}{\varepsilon} = Y_d \equiv -\frac{1}{2} \frac{dC_{ijkl}(d)}{dd} e_{xkl}(\mathbf{u}^{(0)}) e_{xij}(\mathbf{u}^{(0)}) \quad (26)$$

where Y_d is the (macroscopic) damage energy release rate. This relation is entirely deduced from microstructural assumptions, without any assumptions on the scaling of energy. This scaling with ε is naturally appearing in the derivation of the damage equation (26). For evolving damage, the previous relation shows that the microstructural length ε makes the link between the surface energy dissipated during micro-crack propagation and damage energy dissipated per unit volume. This energy scaling property will assure the presence of the internal length ε in the damage laws.

Using (26) from the micro-crack evolution laws (23) and (24), we deduce the damage law

$$\dot{d} = \frac{1}{\varepsilon} \bar{v}(\varepsilon Y_d) \quad (27)$$

$$\mathcal{D}_d \equiv Y_d \dot{d} \geq 0 \quad (28)$$

We remark the presence of the material length in the damage model given by the relations (27) and (28).

To complete the proof of the thermodynamic compatibility for the damage model obtained by homogenization, we note that one can introduce the macroscopic free energy function

$$\Psi(e_{xij}, d) \equiv \frac{1}{2} C_{ijkl}(d) e_{xkl}(\mathbf{u}^{(0)}) e_{xij}(\mathbf{u}^{(0)}) \quad (29)$$

which becomes a potential for the associated thermodynamical “forces” (Lemaitre and Desmorat, 2005):

$$\Sigma_{ij} = \frac{\partial \Psi}{\partial e_{xij}}; \quad Y_d = -\frac{\partial \Psi}{\partial d} \quad (30)$$

Combination of (25) and (26) yields to the expression of the stress intensity factor

$$K_I = \left(-\frac{\varepsilon E}{2(1 - \nu^2)} \frac{\partial C_{ijkl}(d)}{\partial d} e_{xkl}(\mathbf{u}^{(0)}) e_{xij}(\mathbf{u}^{(0)}) \right)^{\frac{1}{2}} \quad (31)$$

Substituting K_I of Eq. (31) in the composite subcritical law (11) and considering the definition of the damage variable $d = \frac{l}{\varepsilon}$ gives us the following macroscopic damage law in the form of (27):

$$\dot{d} = \frac{1}{\varepsilon} \left(\frac{ab \exp(S_1 K_I)}{a \exp(S_1 K_I) + b} + c \exp(S_3 K_I) \right) \quad (32)$$

where K_I is expressed according to macroscopic variables through Eq. (31). In this way, Eq. (32) becomes a macroscopic damage equation which is coupled with the equilibrium equation (22).

This damage equation accounts not only for the rate effect but also for the size effect. Indeed, according to Eq. (31), the stress intensity factor included in the damage equation (32) depends on the size of the periodic structure, ε , and on the damage variable d (being the ratio between the crack length l and ε). So, the developed model reflects the nonlinear, time- and size-dependent effect on the damage behaviour of material, as commonly observed in experiment.

5. Numerical simulations

The time-dependent behaviour of materials can be underlined by means of various laboratory tests. In particular, quasi-static compression tests, creep tests or relaxation tests may point out the same time-dependent properties under different stress and strain conditions. In this section, numerical results are presented

for these tests. We simulate the local macroscopic elastic damage response. The set of material parameters that have been used in the simulations are reported in Table 1. The simulations have been made considering tension loading under strain- or stress-controlled conditions in the vertical direction while the horizontal direction is free of stress. Plane-strain condition is considered in the third direction. All the simulations start from an undamaged material ($d^0 = 1 \times 10^{-9} \approx 0$).

5.1. Numerical integration method

For the analysis of the homogenized response in a macroscopic point, the input of this system of Eqs. (20) and (32) is the macroscopic stress $\Sigma_{ij}^{(0)}$ or strain $e_{xkl}(\mathbf{u}^{(0)})$, depending on the physical problem to be studied. Due to the dependency of the elastic modulus C_{ijkl} on the damage variable d and the form of the damage energy release rate (26) used to calculate the stress intensity factors, the problem is highly non-linear. For each time step, the stress-controlled problem is solved by an iterative procedure as follows:

1. Initialization ($n = 1$), $d_0^t = d^{t-1}$ (if $t = 0$, $d = d^0$).
2. $C_{ijkl} = C_{ijkl}(d_{n-1}^t)$.
3. Prediction of the macroscopic strain: $e_{xij,n-1} = C_{ijkl}^{-1}(d_{n-1}^t) \Sigma_{ij}^{(0)}$.
4. Determination of the stress intensity factor: $K_I = K_I(C_{ijkl}(d_{n-1}^t))$.
5. Update of the damage: $\dot{d} = f(e_{xij,n-1}, C_{ijkl}(d_{n-1}^t))$; $d_n^t = d^{t-1} + \dot{d} \Delta t$.
6. Update of the homogenized coefficient: $C_{ijkl} = C_{ijkl}(d_n^t)$.
7. Calculation of the updated strain: $e_{xij,n} = C_{ijkl}^{-1}(d_n^t) \Sigma_{ij}^{(0)}$.

8. The convergence of the solution is tested: $CONV = \frac{\|\mathbf{e}_n - \mathbf{e}_{n-1}\|^2}{\|\mathbf{e}_n\|^2}$.

- (i) If $CONV \leq Tol$: Return to point 1 with a new time step ($t = t + 1$).
- (ii) If $CONV > Tol$: Return to point 2 with $n = n + 1$.

where n is the iteration step, t is the time step number, Δt is the size of the time step, d^0 is the initial damage variable and Tol is the tolerance taken as 10^{-5} .

We note that, because the damage energy release rate (26) is written in term of macroscopic strain, this procedure becomes trivial in the strain control case.

5.2. Loading at constant strain rate

Under tension tests at constant strain rate, the micro-cracking depends not only on the strain level, that controls the stress intensity factor at the crack tips, but also on time. The response of the model under a vertical tension rate of 10^{-8} s^{-1} is illustrated in Fig. 4 in terms of stress, damage and stress intensity factor evolutions with time. Also plotted is the velocity of crack propagation related to the stress intensity factor through the subcritical law. As long as the vertical strain increases, the stress intensity factor increases. So doing, the regime of crack propagation starts in region I until K_I reaches K_T . At the beginning of this region, the rate of crack propagation is low, i.e. the damage increases slowly and the loss of rigidity is relatively limited. So, at the beginning of the test, the behaviour appears quasi linear. Bold lines reproduce the response of the material for the material parameters reported in Table 1. For such parameters, when the stress intensity factor

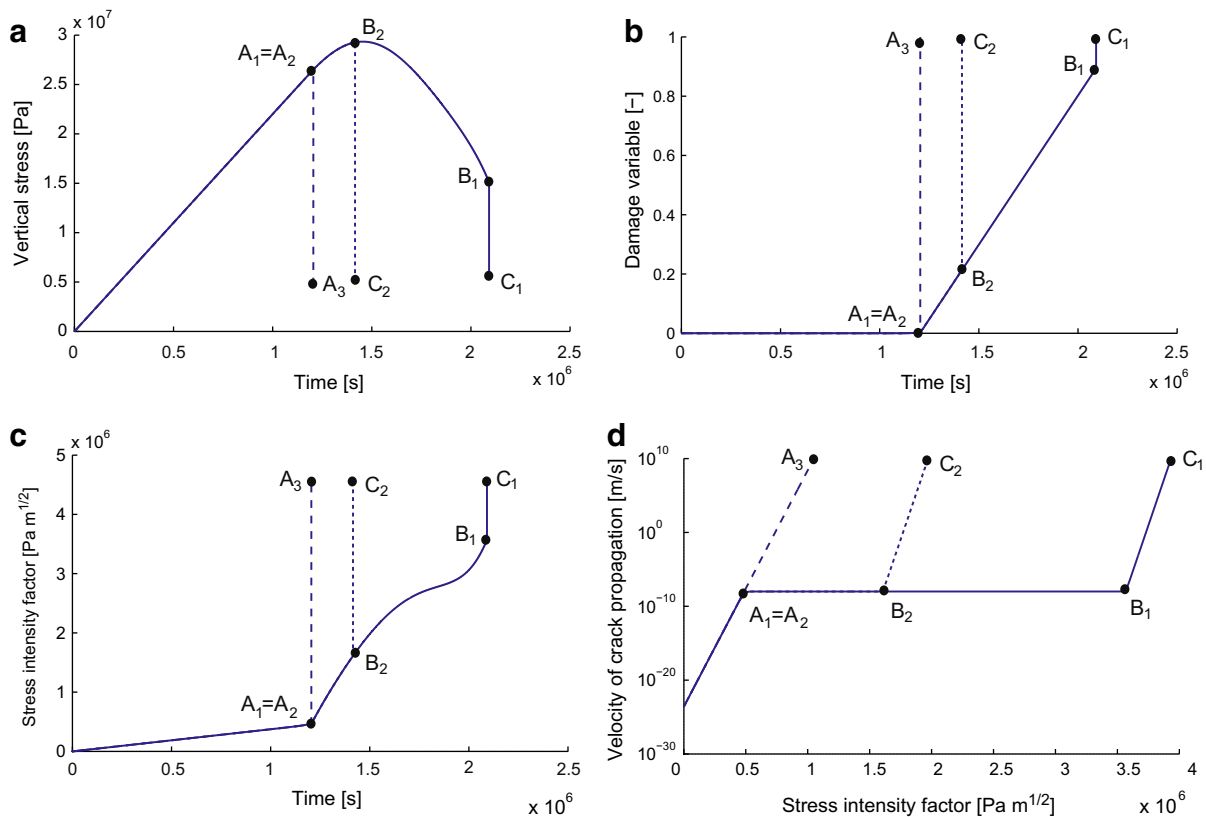


Fig. 4. Numerical results of a vertical tension test at constant strain rate. Evolution of (a) stress, (b) damage variable, (c) stress intensity factor with time and (d) velocity of crack propagation with respect to the stress intensity factor. The three damage regimes are separated by letters A, B and C. The different curves correspond to different amplitudes of the plateau of region II.

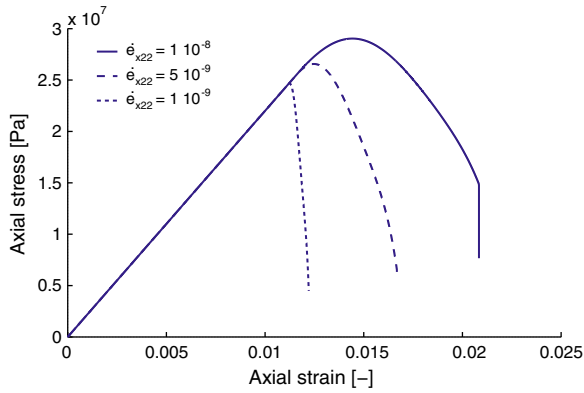


Fig. 5. Effect of the strain rate of loading on the behaviour of materials subject to a vertical tension test at constant strain rate.

overpasses K_T (in point A_1), the rate of crack propagation becomes independent of the loading level, as seen in Fig. 4d between points A_1 and B_1 . That regime is characterized by a constant rate of damage propagation inducing a progressive loss of material rigidity, that creates the peak and the post-peak softening behaviour observed in Fig. 4a. Finally, when K_I reaches K_m (at point B_1), a sudden failure appears up to coalescence of micro-cracks ($d = 1$, point C_1). This numerical simulation clearly shows the trimodal behaviour of the crack growth rate with respect to the stress intensity factor at the crack tips. So, the problem is treated completely from crack initiation (usually in region I) toward constant rate of crack propagation (region II) leading to failure (in region III).

The region II induces a ductile behaviour. Indeed, that regime is mainly controlled by the diffusion rate of the reactive species to crack tips which cannot diffuse faster than a given value. It avoids a dramatic increase of the crack velocity, producing a ductile macroscopic response of the material. On the contrary, if the diffusion rate of the reactive species is unlimited, $v_{(2)}$ tends to infinity and the behaviour remains in region I until reaching a brittle failure (point A_3 in Fig. 4). Also, the extension of the region II can be limited by a lower critical value of the stress intensity factor which control the behaviour in region III. Decreasing the zero stress activation energy in region III from 2×10^{-18} to 1×10^{-18} , the region III appears (point B_2 in Fig. 4) for lower value of the stress intensity factor and the extension of the plateau of region II is lower. As a consequence, the failure is also more brittle (point C_2).

Because of the time-dependent behaviour of materials, the strength is affected by the strain rate of loading $\dot{\epsilon}_{x22}$. Usually, faster is the loading and higher is the strength. When $\dot{\epsilon}_{x22}$ is sufficiently low, the subcritical micro-cracking in the material has enough time to develop inducing a decrease of the material strength. On the contrary, a fast loading avoid the development of delayed cracking which enhances the strength. The developed model reproduces this effect as shown in Fig. 5. In this example, a loading 10 times slower decreases the strength of about 15% (from 29 MPa to 24.5 MPa).

The variation of the zero stress activation energy of region I, U'_{01} , translates the curve $(\log v_{(1)} - K_I)$ without changing its slope. For increasing value of U'_{01} , the velocity of crack propagation decreases for a same K_I and the transition between regions I and II (K_T) is shifted to the right. So, when U'_{01} decreases, K_T is tending to K_m and region II is progressively disappearing. The distance between

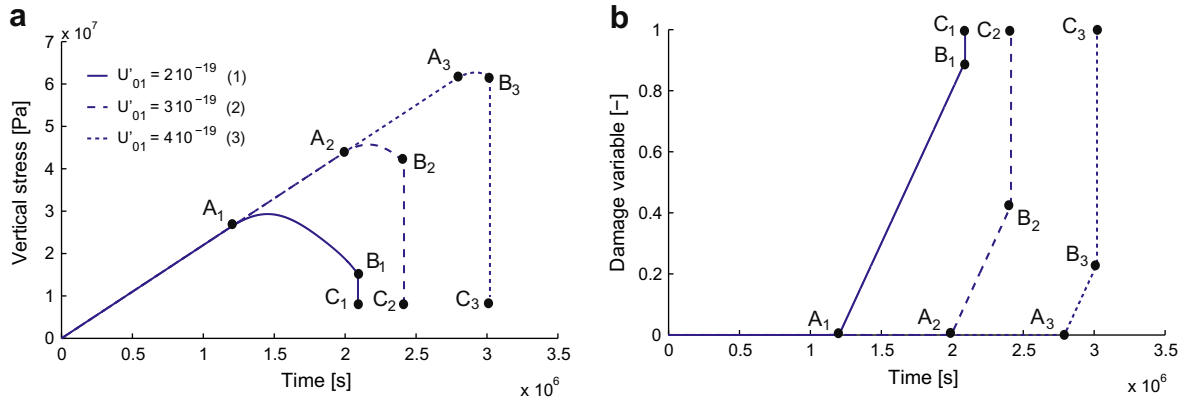


Fig. 6. Effect of the zero stress activation energy of region I on numerical results of a vertical tension test at constant strain rate. Evolution of (a) stress, (b) damage variable and with time.

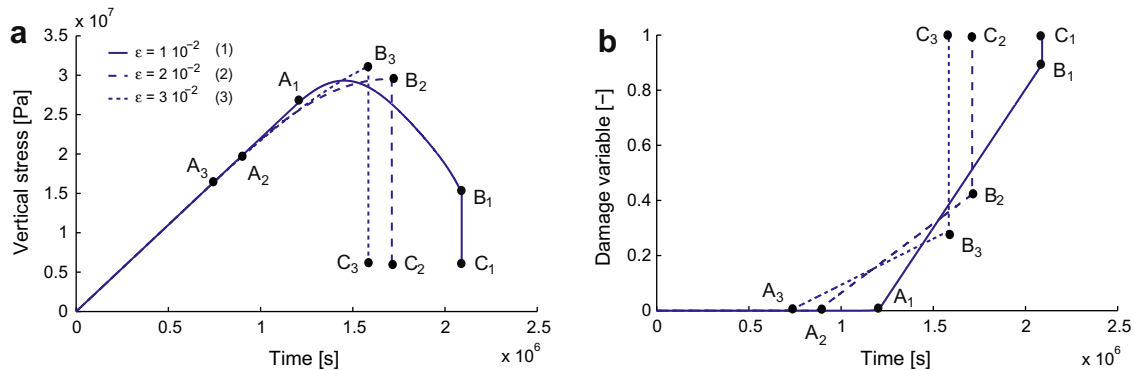


Fig. 7. Effect of the internal length on numerical results of a vertical tension test at constant strain rate. Evolution of (a) stress and (b) damage variable with time.

points A and B decreases which makes the behaviour more brittle (Fig. 6).

In Fig. 7, the role of internal length variation ε on the response of the tensile test at constant strain rate is shown. The effect of this parameter is twofold. (i) Under a given strain field and a given damage level, the stress intensity factor is proportional to $\varepsilon^{1/2}$ (Eq. (31)). So, the smaller is the microstructure, the lower is the stress concentration at the micro-crack tips. In that sense, the decrease of ε postpones the crack propagation, by increasing the resistance to failure. Fig. 7b shows that the time (e.g. the vertical strain) needed to reach region II (characterized by points A) is increasing when the internal length decrease. (ii) However, the same velocity of micro-crack propagation produces an higher dam-

age rate for smaller microstructure ($\frac{dd}{dt} = \frac{v}{\varepsilon}$). So, the two effects of ε are opposite. The first one postpones the failure while the second one accelerates it which makes that the effect of ε on the peak strength is a complex one.

5.3. Relaxation test

The relaxation test is obtained by keeping a constant strain level. Even if the solicitation is not evolving, the micro-crack may propagate under subcritical conditions until complete failure of the material. Under constant tension loading, the subcritical micro-crack growth produces a progressive decrease of the rigidity as long as the damage state increases. As a consequence, the vertical

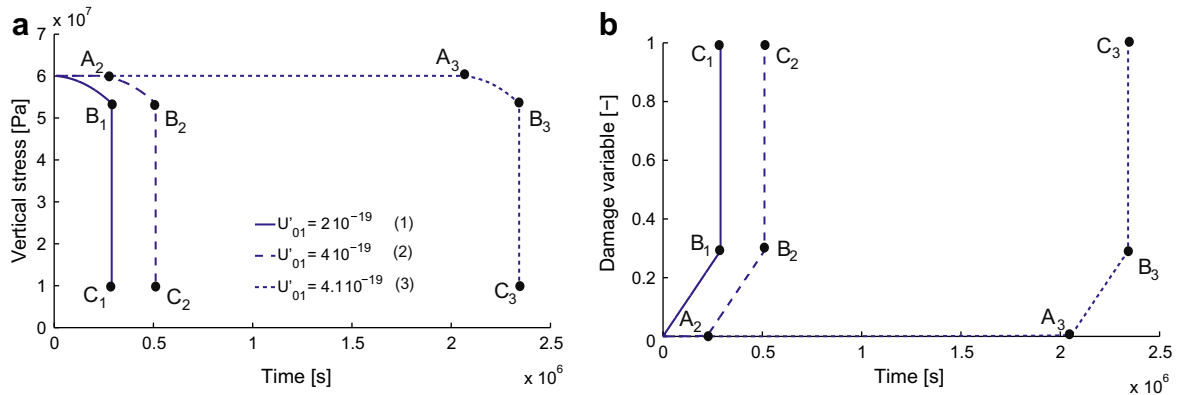


Fig. 8. Effect of the zero stress activation energy of region I on numerical results of relaxation test. Evolution of (a) stress and (b) damage variable with time.

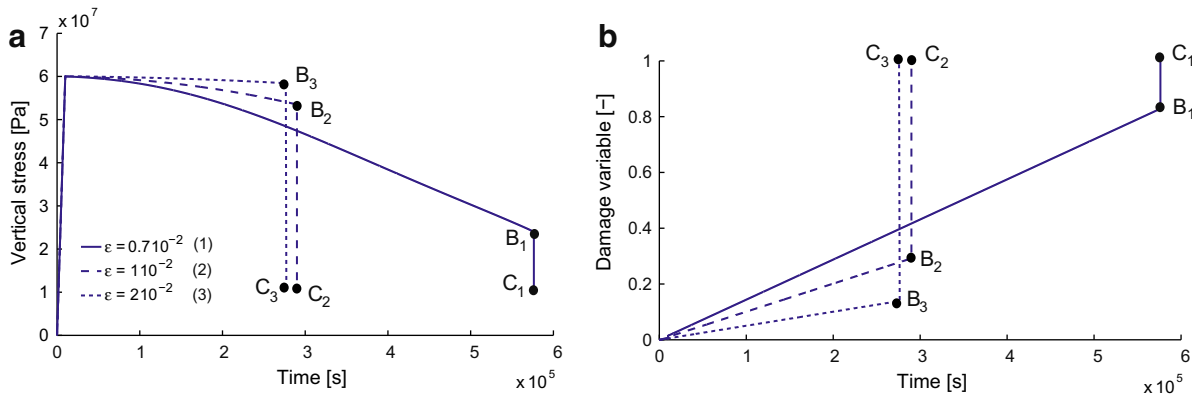


Fig. 9. Effect of the internal length on numerical results of relaxation test. Evolution of (a) stress and (b) damage variable with time.

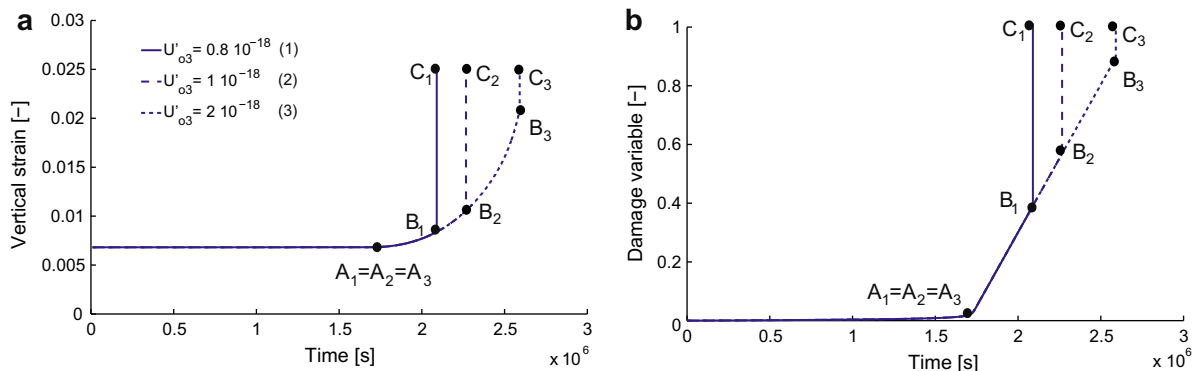


Fig. 10. Effect of the zero stress activation energy of region III on numerical results of creep test. Evolution of (a) stress and (b) damage variable with time.

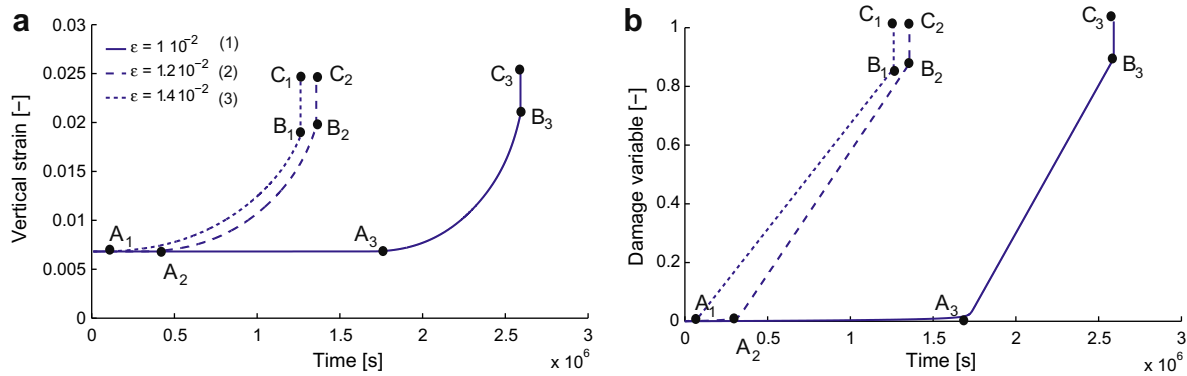


Fig. 11. Effect of the internal length on numerical results of creep test. Evolution of (a) stress and (b) damage variable with time.

stress is gradually relaxing with time, towards the ultimate state, when the micro-cracks coalesce and the rigidity tends to zero. Under a constant vertical strain $\epsilon_{x22}(\mathbf{u}^{(0)}) = 0.0273$, Figs. 8 and 9 show, respectively, the effect of the variations U'_{01} and ϵ on the vertical stress decrease in parallel with the damage increase. Instantaneously, the applied vertical strain generates a vertical stress of around 60 MPa that is the stress produced by the applied strain for the undamaged material. For $U'_{01} = 2 \times 10^{-19}$, the zero stress activation energy of region I is so low that the vertical strain of $\epsilon_{x22}(\mathbf{u}^{(0)}) = 0.0273$ produces a stress intensity factor at the crack tips, K_I , higher than K_T which makes that the crack propagation starts in region II. However, for higher U'_{01} , K_T is shifted toward higher K_I and the crack propagation starting in region I and the three distinct regions are now visible with transition in points A, B and C (Fig. 8).

As explained in the previous section, the increase of ϵ decreases the rate of damage propagation in region II (before points B in Fig. 9b) and pushes forward the transition between region II and III (points B).

5.4. Creep test

As for relaxation tests, under the condition of creep tests (i.e. keeping a constant stress level), the failure is not governed by the maximal stress that the material may sustain but rather by the time needed for the micro-cracks to propagate under subcritical conditions. Figs. 10 and 11 depict the effect of the variations of U'_{03} and ϵ on the vertical creep strain in parallel with the damage increase under a constant tensile vertical stress $\Sigma_{22}^{(0)} = 15$ MPa. After an instantaneous vertical strain corresponding to the short-term response of the material, the time effect makes damage variable increase, successively in regions I, II and III. The lower is U'_{03} and the faster is the transition between regions II and III (points B in Fig. 10). The modification of U'_{03} does not affect region I. The effect of the variation of ϵ (Fig. 11) is similar to the ones explained in the two previous sections.

6. Conclusions

The subcritical growth of micro-cracks is responsible of the time-dependent behaviour of many quasi-brittle materials. The subcritical propagation criterion has been applied for cracks at the micro-scale and up-scaled by the asymptotic homogenization procedure. A time-dependent macroscopic damage model has been deduced and the stress-strain response of materials, depending on time, has been obtained in a macroscopic point. The damage law contains a microstructural length allowing for the prediction of size effects.

The subcritical law considers trimodal behaviour of crack propagation with time. The behaviour within those three regions have been interpreted in terms of physical processes at the crack tip level, according to Salganik et al. (1997), through microstructural material parameters.

As long as the micro-cracks grow due to the combined effect of time and high stresses at the crack tips, the damage increases, the global rigidity of the material decreases and the subcritical crack propagation crosses the three regions of failure behaviour, from crack initiation to coalescence of cracks upon rupture. With the assumption of trimodal behaviour of crack propagation, there is no stress (or strain) threshold for the activation of the subcritical crack growth. As a consequence, in theory, the material creep damage may occur even at very low stress (or strain) level. However, for infinitely slow strain rate (for controlled strain rate test) or infinitely low constant stress or strain level (for creep or relaxation tests), the time of failure become infinite.

The evolution of rigidity with respect to damage has been quantified by the means of a series of finite element simulations on a unit cell with different crack lengths. Numerical simulations of the effective elasto-damage response have shown the ability of the model to reproduce the time-dependent behaviour of materials. In particular, tensile test at constant strain rate, creep and relaxation tests have been simulated. A parametric studies of the effect of the size of the micro-structure and the level of activation energies has been carried out. They show the capacity of the model to be adapted for a large range of different material behaviours. For each simulation, the trimodal behaviour has been emphasized.

References

- Abou-Chakra Guery, A., Cormery, F., Shao, J.F., Kondo, D., 2009. A multiscale modeling of damage and time-dependent behavior of cohesive rocks. *Int. J. Numer. Anal. Meth. Geomech.* 33, 567–589.
- Anderson, O., Grew, P., 1977. Stress corrosion theory of crack propagation with applications to geophysics. *Rev. Geophys. Space Phys.* 15, 77–104.
- Atkinson, B., Meredith, P., 1987. The theory of subcritical crack growth with applications to minerals and rocks. In: *Fracture Mechanics of Rocks*. Academic Press, New York, pp. 111–166.
- Benssousan, A., Lions, J., Papanicolaou, G., 1978. *Asymptotic Analysis for Periodic Structures*. Kluwer Academic Publisher, Amsterdam.
- Betten, J., 2002. *Creep Mechanics*. Springer, Berlin.
- Challamel, N., Lanos, C., Casandjian, C., 2005. Creep damage modelling for quasi-brittle materials. *Eur. J. Mech. A/Solids* 24, 593–613.
- Charles, R., 1958. Dynamic fatigue of glass. *J. Appl. Phys.* 29, 1657–1662.
- Cristescu, N., Hunsche, U., 1998. *Time-Effects in Rock Mechanics*. Wiley, England.
- Dartois, S., Nadot-Martin, C., Halm, D., Dragon, A., Fanget, A., 2009. Discrete damage modelling of highly-filled composites via a direct multiscale morphological approach. *J. Multisc. Model.* 1.
- Dascalu, C., 2009. A two-scale damage model with material length. *C.R. Mecanique* 337, 645–652.
- Dascalu, C., Bilbie, G., 2007. A multiscale approach to damage configurational forces. *Int. J. Fract.* 147, 285–293.

- Dascalu, C., Bilbie, G., Agiasofitou, E., 2008. Damage and size effect in elastic solids: a homogenization approach. *Int. J. Solid Struct.* 45, 409–430.
- François, B., Dascalu, C., submitted for publication. A two-scale time-dependent damage model based on non-planar growth of micro-cracks.
- Freiman, S., 1984. Effects of chemical environments on slow crack growth in glasses and ceramics. *J. Geophys. Res.* 89, 4072–7076.
- Freund, L.B., 1998. *Dynamic Fracture Mechanics*. Cambridge University Press, Cambridge.
- Leguillon, D., Sanchez-Palencia, E., 1982. On the behavior of a cracked elastic body with (or without) friction. *J. Mech. Theor. Appl.* 1, 195–209.
- Lemaitre, J., Desmorat, R., 2005. *Engineering Damage Mechanics: Ductile, Creep, Fatigue and Brittle Failures*. Springer, Berlin.
- Main, I., 2000. A damage mechanics model for power-law creep and earthquake aftershock and foreshock sequences. *Geophys. J. Int.* 142, 151–161.
- Meredith, P., Atkinson, B., 1985. Fracture toughness and subcritical crack growth during high-temperature tensile deformation of westerly granite and black gabbro. *Tectonophysics* 39, 33–51.
- Miura, K., Okui, Y., Horii, H., 2003. Micromechanics-based prediction of creep failure of hardrock for long-term safety of high-level radioactive waste disposal system. *Mech. Mater.* 35, 587–601.
- Munt, D., Fett, T., 2001. *Ceramics: Mechanical Properties, Failure Behavior, Materials Selection*. Springer, Berlin.
- Nadot, C., Dragon, A., Trumel, H., Fanget, A., 2006. Damage modelling framework for viscoelastic particulate composites via a scale transition approach. *J. Theor. Appl. Mech.* 44, 553–583.
- Nara, Y., Kaneko, K., 2006. Sub-critical crack growth in anisotropic rock. *Int. J. Rock Mech. Min. Sci.* 43, 437–453.
- Okui, Y., Horii, H., 1997. Stress and time-dependent failure of brittle rocks under compression: a theoretical prediction. *J. Geophys. Res.* 102 (B7), 14869–14881.
- Pietruszczak, S., Lydzba, D., Shao, J.F., 2004. Description of creep in inherently anisotropic frictional materials. *J. Eng. Mech.* 6, 681–690.
- Ruckert, C.O.F.T., Tarpani, J.R., Bose Filho, W.W., Spinelli, D., 2006. On the relation between micro- and macroscopic fatigue crack growth rates in aluminum alloy AMS 7475-T7351. *Int. J. Fract.* 142, 233–240.
- Salganik, R., Rapoport, L., Gotlib, V., 1997. Effect of structure on environmentally assisted subcritical crack growth in brittle materials. *Int. J. Fract.* 87, 21–46.
- Sanchez-Palencia, E., 1980. *Non-homogeneous Media and Vibration Theory*. Lecture Notes in Physics, vol. 127. Springer, Berlin.
- Scholz, C.H., 1972. Static fatigue of quartz. *J. Geophys. Res.* 77, 2104–2114.
- Taylor, R., 2008. *FEAP – A Finite Element Analysis Program – Version 8.2 – User Manual*.
- Wiederhorn, S., Bolz, L., 1970. Stress corrosion and static fatigue of glass. *J. Am. Ceram. Soc.* 53, 543–548.